CHEMICAL REVIEWS

Review

pubs.acs.org/CR

Protein Allostery and Conformational Dynamics

Jingjing Guo[†] and Huan-Xiang Zhou*[,‡]

[†]School of Chemistry and Chemical Engineering, Henan Normal University, Xinxiang, Henan 453007, People's Republic of China
[‡]Department of Physics and Institute of Molecular Biophysics, Florida State University, Tallahassee, Florida 32306, United States

ABSTRACT: The functions of many proteins are regulated through allostery, whereby effector binding at a distal site changes the functional activity (e.g., substrate binding affinity or catalytic efficiency) at the active site. Most allosteric studies have focused on thermodynamic properties, in particular, substrate binding affinity. Changes in substrate binding affinity by allosteric effectors have generally been thought to be mediated by conformational transitions of the proteins or, alternatively, by changes in the broadness of the free energy basin of the protein conformational state without shifting the basin minimum position. When effector binding changes the free energy landscape of a protein in conformational space, the change affects not only thermodynamic properties but also dynamic properties, including the amplitudes of motions on different time scales and rates of conformational transitions. Here we assess the roles of conformational dynamics in allosteric regulation. Two cases are highlighted where NMR spectroscopy and molecular dynamics simulation have been used as complementary approaches to identify residues possibly involved in allosteric communication. Perspectives on contentious issues, for example, the relationship between picosecond−nanosecond local and microsecond−millisecond conformational exchange dynamics, are presented.

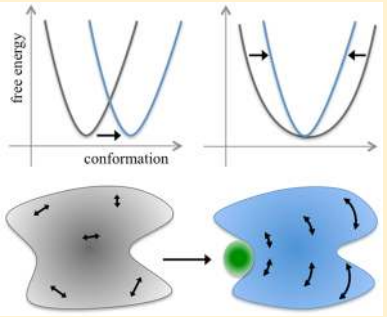

CONTENTS

1. INTRODUCTION

The functions of many proteins are regulated through allostery, whereby effector binding at a distal site changes the functional activity (e.g., substrate binding affinity or catalytic efficiency) at the active site (Figure 1a). Since the introduction of the word "allosteric" by Monod and Jacob[1] in 1961, allosteric studies have mainly focused on thermodynamic properties, in particular, substrate binding affinity. Changes in substrate binding affinity by allosteric effectors have generally been thought to be mediated by conformational transitions of the proteins (Figure 1b, left), as illustrated by Monod, Wyman, and Changeux (MWC) using the T to R quaternary conformational transition of hemoglobin.[2] An alternative idea, considered by Wyman and Allen[3] as early as 1951 and popularized by Cooper and Dryden,[4] is that an allosteric effector may simply change the broadness of the free energy basin of the protein conformational state, rather than shifting the basin to a distinctly different region in conformational space (Figure 1b, right). This type of allostery, known as entropically driven, has gained considerable attention, as many allosteric proteins show only subtle structural differences before and after binding effectors (see ref 5 for a reappraisal of such structural differences). Recently a change in the broadness (as opposed to the minimum position) of the free energy basin of the ligand-binding domain was proposed to underlie the partial agonism of a ligand-gated ion channel.[6,7] When effector binding changes the free energy landscape of a protein in conformational space, the change affects not only thermodynamic properties but also dynamic properties, including the amplitudes of motions on different time scales (Figure 1c) and rates of conformational transitions.

Whereas the functional consequences (e.g., an increase in substrate binding affinity) of allosteric binding can be directly measured, the mechanisms of action are concluded with the help of inference and simplification. Allosteric mechanisms have been delineated by two types of pathways. The first type, referred to as transition pathway here, connects the end states of an allosteric transition, for example, a conformational change upon allosteric binding (Figure 2). In the induced-fit pathway,[8]

Special Issue: Protein Ensembles and Allostery

Received: October 7, 2015
Published: February 15, 2016

DOI: 10.1021/acs.chemrev.5b00590
Chem. Rev. 2016, 116, 6503−6515

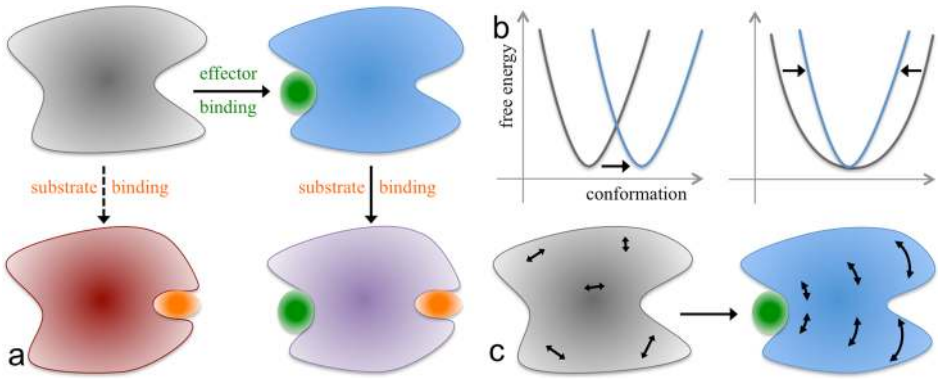

Figure 1. Conformational and dynamic effects of allosteric binding. (a) Binding of an effector at the allosteric site primes the binding of the substrate at the active site, and consequently the thermodynamic or kinetic properties of the latter binding are different from those in the absence of the effector. (b) Allosteric binding may result in a change in (left) conformational state, as signified by the movement of the corresponding free energy basin from one region to another region in conformational space, or (right) broadness of the free energy basin. (c) Conformation dynamics may be changed as well, for example, from uncorrelated, fast (e.g., subnanosecond) motions in the apo form to correlated, slow (e.g., > microsecond) motions in the effector-bound form. Internal motions are represented by double-headed arrows.

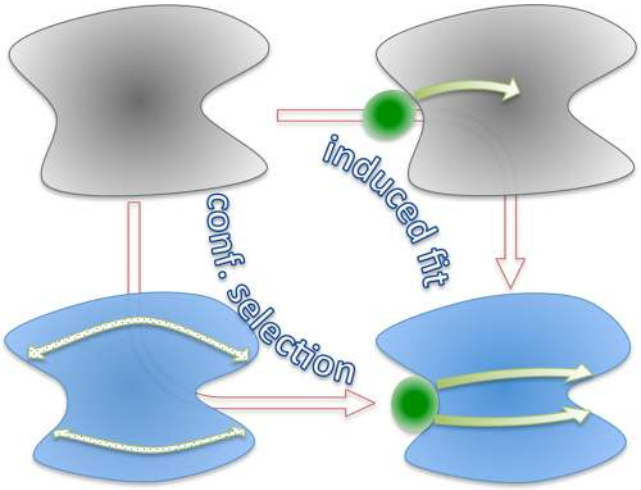

Figure 2. Transition pathways connecting the end states of allosteric binding and communication pathways from the allosteric site to the active site. The allosteric transition illustrated here is a conformational change, with apo and bound conformations represented by gray and blue shading, respectively. Transition pathways, indicated by brown arrows, are mainly concerned with kinetic intermediates: the induced-fit pathway passes through the intermediate in which the effector is loosely bound with the protein in the apo conformation, whereas the conformational-selection pathway passes through the intermediate in which the apo protein adopts the bound conformation. Communication pathways, indicated by green arrows, are concerned with intermediate residues through which the allosteric site is coupled with the active site. The two types of pathways thus differ in their emphases but are not orthogonal to each other. In the induced-fit transition pathway, the conformational change initiated by loose effector binding propagates to the active site while the effector consolidates its binding. In the conformational-selection pathway, stabilization of the bound conformation starts at the allosteric site and propagates to the active site.

the allosteric transition proceeds with the effector first binding loosely to the protein in the apo conformation and the protein then switching to the bound conformation. Alternatively, in the conformational-selection (also known as population-shift) pathway,[9,10] the apo protein first switches to the bound conformation and the effector then binds. There has been much debate about transition pathways in defining allosteric mechanism.[11,12] However, the historical debate between the MWC model[2] and the model of Koshland, Nemethy, and Filmer (KNF),[13] though sometimes presented as representing conformational selection and induced fit, respectively, is not really about transition pathways. Rather, this debate is about the origin of binding cooperativity in hemoglobin (and other oligomeric proteins). MWC attributed the free energy of cooperation to a *concerted* change in quaternary structure but KNF to *sequential* changes in tertiary structures that affect intersubunit physical interactions. Another point of contention is whether the detection of a minor population of conformations characteristic of the effector-bound form when the protein is free of the effector can be taken as proof of the conformational-selection pathway. As has been argued,[11,14] every conformation has an equilibrium probability according to the Boltzmann distribution; whether bound conformations can be detected depends on the sensitivity of the experimental probe and therefore should not dictate the mechanism of allosteric transition.

In any event, strictly speaking, transition pathways are irrelevant when thermodynamic properties of allostery are considered. That is because, fundamentally, thermodynamic properties depend only on end states, not on transition pathways connecting them. By contrast, kinetic properties do depend on transition pathways.[15] In particular, the relative contributions of induced-fit and conformational-selection pathways to the rate of protein−effector binding can be measured.[14,16] The relative contributions of the two pathways depend on both intrinsic factors, in particular the rates of conformational transition,[14,17] and extrinsic factors, in particular effector concentration.[14,16] With increasing rates of conformational transition or effector concentration, the induced-fit pathway becomes dominating.

The second type of pathway concerns the communication between the allosteric site and the active site (Figure 2). Perutz[18] presented an early model of communication pathway for hemoglobin, based on structure comparison and structure−function correlation. In this model, oxygen binding to the T conformation triggers movement of the iron into the heme plane, realignment of the neighboring helices, and breakage of intersubunit salt bridges, thereby shifting the quaternary equilibrium toward the R conformation (in line with the MWC model; see refs 19 and 20 for subsequent development

DOI: 10.1021/acs.chemrev.5b00590
Chem. Rev. 2016, 116, 6503−6515

of allosteric models for hemoglobin). Many workers (though with notable exceptions)[21] presume that networks of residues that exhibit spatial correlations in conformations or temporal correlations in motions mediate the communication between allosteric and active sites. One may identify these communication pathways by comparing residue-specific differences in conformations and dynamics between the apo form, effector-bound form, and ternary complex with both effector and substrate bound. NMR spectroscopy has now been established as a powerful tool for characterizing allosteric communication, due to its ability to provide atomic-level information on chemical environment and on picosecond−nanosecond local (backbone or side chain) and microsecond−millisecond conformational exchange dynamics.[22−28]

In principle, long molecular dynamics simulations can provide all the details regarding the communication between allosteric and active sites, and simulations longer than a microsecond are beginning to shed light on communication mechanisms.[29−31] Computational studies are still mostly based on submicrosecond simulations or on contact analysis or elastic network modeling of static crystal structures.[32] Notably, allosteric communication has been assumed to involve evolutionarily conserved[33] or positionally correlated[34] networks of residues. The complementarity of computational and experimental approaches, NMR spectroscopy in particular, in studying allostery can be easily appreciated.

In recent years there has been intense interest in the potential roles of conformational dynamics in allosteric regulation. In referring to entropically driven allostery, a number of workers have used the word dynamic (e.g., ref 4), but what was really meant is just that proteins are not static but, under equilibrium fluctuation, can sample an ensemble of conformations.[20,35] The extent of conformational sampling in a (meta)stable state is measured by conformational entropy, which, like all thermodynamic properties, is microscopically determined by the shape of the free energy basin in conformational space. Beyond thermodynamic properties, dynamic properties characterizing time-dependent processes are also observables, including the time scales, amplitudes, and spatial−temporal correlations of internal motions as well as rates of conformational transitions. Microscopically, dynamic properties are governed by the equations of motion and are dictated by not only free energy basins but also barriers, along with dynamic parameters (e.g., effective diffusion coefficients).

Given the latter strict sense of the word dynamic, there may be three views on conformational dynamics as it relates to allostery. The first view is that allosteric regulation should be limited to thermodynamic properties only; any effect on conformational dynamics is a mere byproduct.[36] For example, an allosteric effector may increase the substrate binding affinity by reducing side-chain flexibility, leading to a lower conformational entropic cost or preorganization of the active site.[25,37] As a consequence, the amplitudes of the picosecond−nanosecond orientational dynamics of the side chains may also be reduced.

The second view is that, even if conformational dynamics does not dictate the final thermodynamic outcome, characterizing it can lead to a fuller understanding of allosteric regulation.[38] As already noted, the rates of conformational transitions are a key determinant of transition pathways. Conformational dynamics may also be involved in mediating allosteric communication.[24,25,39] Absent such involvement, conformational dynamics may still be helpful in identifying communication pathways, as illustrated by the residues with suppressed subnanosecond side-chain dynamics in the last example.

The third view is that allosteric regulation also extends to kinetic properties, and surely conformational dynamics is a determinant of these properties. In particular, enzyme kinetics is characterized by two parameters, the turnover number k_{cat} and the Michaelis constant K_M. These parameters in turn are determined by the rate constants of the three basic steps of the enzyme-catalyzed reaction: substrate binding, chemical transformation of substrate into product, and product release. Allosteric effectors have been suggested to affect millisecond time scale dynamics implicated in these basic steps and thereby modulate the corresponding rate constants.[40−43]

In this review we aim to assess the roles of conformational dynamics in allosteric regulation. We highlight two proteins for which NMR spectroscopy and molecular dynamics simulation have been used as complementary approaches to identify residues possibly involved in allosteric communication, for example, by following effector-induced changes in dynamic properties or positional correlations. We also present our perspectives on several contentious issues, such as the relationship between picosecond−nanosecond local and microsecond−millisecond conformational exchange dynamics, and on future developments, including designing molecular dynamics simulations to test ideas about allosteric communication.

2. APPROACHES FOR CHARACTERIZING ALLOSTERIC COMMUNICATION

Effector-induced changes in conformational dynamics and positional correlations, probed by NMR spectroscopy and molecular dynamics simulation, respectively, are often used to characterize allosteric regulation. Below we give some basic ideas behind these experimental and computational approaches, hopefully to allow the reader better appreciation of the results to be covered in section 3.

2.1. NMR Relaxation and Conformational Dynamics

Different types of NMR relaxation experiments can report conformational dynamics on different time scales.[44] The magnetization arising from nuclear spins can be decomposed into a longitudinal component (i.e., parallel to the static magnetic field B_0) and a transverse component. In two classical experiments, one observes time-dependent recovery of the equilibrium value of the longitudinal component and time-dependent decoherence of the transverse component. The main mechanisms that contribute to longitudinal and transverse relaxation for a nuclear spin S (e.g., backbone ^{15}N) involve magnetic dipole−dipole interaction (e.g., with backbone amide ^{1}H, referred to as spin I) and chemical shift anisotropy (CSA) of the S spin.[45] These act as time-dependent (due to stochastic molecular motions) perturbations to the Hamiltonian of the S spin. The dipolar contribution depends on the magnitude (r_{IS}) and direction of the internuclear vector, whereas the CSA contribution depends on the magnitude ($\Delta\sigma_S$) of the CSA and orientation of the CSA tensor. For a backbone amide ^{15}N−^{1}H spin pair, the ^{15}N CSA tensor is usually nearly axially symmetric and the symmetry axis is nearly collinear with internuclear vector. Here we assume axial symmetry and collinearity along a unit vector $\mathbf{n}$.

Because of stochastic molecular motions, $\mathbf{n}$ is a randomly fluctuating variable, but the correlation $\langle \mathbf{n}(t)\cdot\mathbf{n}(0)\rangle$, between $\mathbf{n}$ at a given moment and $\mathbf{n}$ a time interval t later, upon averaging

DOI: 10.1021/acs.chemrev.5b00590
Chem. Rev. 2016, 116, 6503−6515

over the time course of the molecule and also over an ensemble of molecules, is a smooth, generally decaying function of t. Both the dipolar and CSA contributions to NMR relaxation can be expressed in terms of the spectral density function, which is a Fourier transform of another time-correlation function of the vector **n**:

$$J(\omega) = \frac{2}{5}\int_0^\infty \langle P_2[\mathbf{n}(t)\cdot\mathbf{n}(0)]\rangle \cos(\omega t)\, dt \quad (1)$$

where $P_2(x) = (3x^2 - 1)/2$. The resulting longitudinal and transverse relaxation rates are

$$R_1 = (d^2/4)[J(\omega_I - \omega_S) + 3J(\omega_S) + 6J(\omega_I + \omega_S)] + c^2 J(\omega_S) \quad (2)$$

$$R_2 = R_1/2 + (d^2/4)[2J(0) + 3J(\omega_I)] + (2c^2/3)J(0) \quad (3)$$

where $d = (\mu_0/4\pi)\hbar\gamma_I\gamma_S\langle r_{IS}^{-3}\rangle$ and $c = \Delta\sigma_S\omega_S/\sqrt{3}$, with μ_0 denoting the vacuum permeability, $\hbar$ denoting reduced Planck's constant, and γ_X and ω_X ($= \gamma_X B_0$) denoting the gyromagnetic ratio and Larmor frequency, respectively, of spin X.

Backbone ^{15}N R_1 and R_2 measurements thus mainly probe orientation dynamics of the NH bond vector and the peptide plane, which typically occur on the picosecond−nanosecond time scale. In a hypothetical situation where the protein is a rigid body, orientation dynamics of the unit vector **n** is solely due to the overall rotational tumbling of the protein (Figure 3a). The time-correlation function is then

$$\langle P_2[\mathbf{n}(t)\cdot\mathbf{n}(0)]\rangle = e^{-t/\tau_c} \quad (4)$$

where $\tau_c = 6D$ is the rotational correlation time, typically on the order of 10 ns, and D is the overall rotational diffusion coefficient (assumed to be isotropic). Generally the unit vector also experiences local orientational dynamics (Figure 3b), which often is much faster than and consequently can be decoupled from the overall rotation, resulting in a time-correlation function[46]

$$\langle P_2[\mathbf{n}(t)\cdot\mathbf{n}(0)]\rangle = e^{-t/\tau_c}[(1 - \mathcal{S}^2)e^{-t/\tau_e} + \mathcal{S}^2] \quad (5)$$

where τ_e is the effective correlation time for local orientational dynamics and $\mathcal{S}^2$, known as the order parameter, reflects the fact that, in the body-fixed reference frame, the local orientational dynamics may not completely randomize the direction of **n**. Upon removing the overall rotation, the time-correlation function decays not to zero but to

$$\mathcal{S}^2 = \frac{4\pi}{5}\sum_{m=-2}^{2} |\langle Y_{2m}(\theta, \phi)\rangle|^2 \quad (6a)$$

$$= \frac{3}{2}\sum_{\alpha,\beta} \langle n_\alpha n_\beta\rangle^2 \quad (6b)$$

where $Y_{2m}(\theta,\phi)$ are spherical harmonics and θ, ϕ, and n_α are the polar and azimuthal angles and Cartesian components, respectively, of the unit vector **n** in the body-fixed frame. By using eq 5 to fit R_1 and R_2 data, one obtains information on the time scale (i.e., t_e) and amplitude (i.e., $1 - \mathcal{S}^2$) of the fast local dynamics. The order parameter can also be directly calculated from molecular dynamics simulations according to eq 6b.[47,48]

As illustration (Figure 3b), consider the local orientational dynamics that is modeled as diffusion in a cone spanning a polar angle θ_0. Evaluation of eq 6a leads to[46]

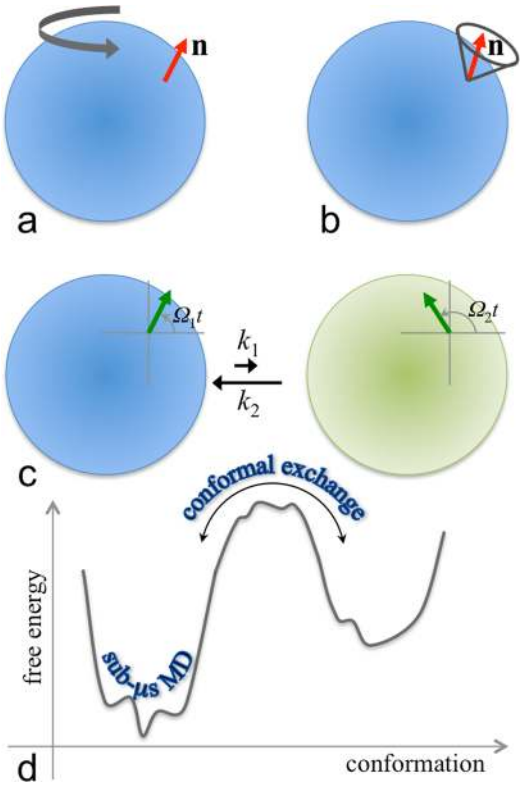

Figure 3. Different types of conformational dynamics. (a) Overall rotational diffusion. Unit vector **n** is assumed to be rigidly attached to the protein, represented by a sphere with blue shading. (b) Local orientational dynamics of **n**, illustrated here as diffusion in a cone, in the body-fixed frame. (c) Conformational exchange between a major state (shaded blue) and a minor state (shaded green). The magnetization (green arrow) precesses at different frequencies in the two states, resulting in dephasing. (d) Conformational sampling on different time scales. Submicrosecond molecular dynamics simulations sample local fluctuations within a single conformational state (or substate therein). Transitions between conformational states require nonlocal correlated motions and cross high free energy barriers, typically occurring on the microsecond−millisecond time scale.

$$\mathcal{S} = (\cos^2\theta_0 + \cos\theta_0)/2 \quad (7)$$

The conformational entropy associated with motion in the cone is

$$S = k_B \ln(1 - \cos\theta_0) \quad (8)$$

By eliminating $\cos\theta_0$, one can directly relate the order parameter to conformational entropy[49,50]

$$S = k_B \ln(3 - \sqrt{1 + 8\mathcal{S}}) \quad (9)$$

where k_B is Boltzmann's constant. Summing the entropies derived from order parameters at different sites in the protein provides a measure of the total conformational entropy. If these calculations are done for the apo and effector-bound forms, the difference can be interpreted as the effector-induced change in protein conformational entropy.[51]

If the S spin can stochastically exchange between two chemical environments (labeled 1 and 2), as occurs when the protein switches between two conformations, the exchange will contribute to dephasing of the transverse magnetization and hence enhance R_2, because spins in the two environments have different precession frequencies (Figure 3c). Relative to the difference $\Delta\nu$ between the resonance frequencies ν_1 and ν_2 in

DOI: 10.1021/acs.chemrev.5b00590
Chem. Rev. 2016, 116, 6503−6515

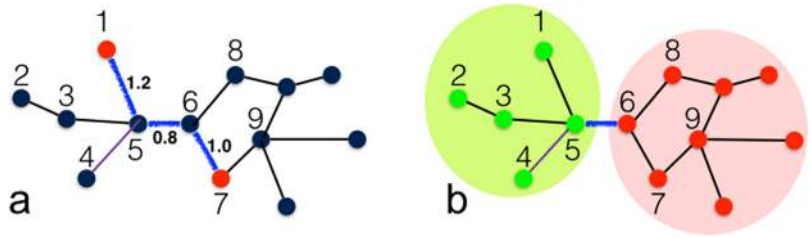

Figure 4. A protein represented as a weighted graph. (a) Shortest path between two nodes 1 and 7, composed of three connected edges shown in blue. Each edge (indicated by a line between two nodes) is assigned a path length (e.g., eq 16 or 17). The path lengths of the three blue edges are shown. Summing over the individual path lengths, the total length of the shortest path is 3.0. (b) The nodes are partitioned into two communities, one with green nodes inside a lime oval and one with red nodes inside a pink oval. An edge between nodes 5 and 6 links the two communities; these nodes are known as critical nodes.

the two environments, the exchange rate k_{ex} (sum of forward and backward transition rates k_1 and k_2) falls into three regimes. In the fast-exchange regime (i.e., $k_{ex} \gg 2\pi\Delta\nu \equiv \Delta\omega$), the NMR spectrum of spin S has a single peak, positioned at the population average of ν_1 and ν_2. With enhancement by chemical exchange, the transverse relaxation rate becomes

$$R_2 = \bar{R}_2^{\,0} + p_1 p_2 \Delta\omega^2 / k_{ex} \tag{10}$$

where $\bar{R}_2^{\,0}$ is the population average of the transverse relaxation rates in the two environments when exchange is absent and p_1 and p_2 are equilibrium population fractions in the two environments. In the slow-exchange regime (i.e., $k_{ex} \ll \Delta\omega$), the NMR spectrum of spin S has two peaks, positioned at ν_1 and ν_2, and the transverse relaxation rates in the two environments are increased by k_1 and k_2, respectively. In the intermediate-exchange regime, the two peaks coalescence, with a broadened line shape. This exchange broadening can often lead to loss of NMR signal. Hence, just like R_2 values that are higher than can be accounted for by overall rotational tumbling and local orientational dynamics, broadened line shapes and unobserved resonances are often interpreted as indicating microsecond−millisecond conformational exchange. However, spin relaxation experiments are generally not suited for quantitative characterization of conformational exchange kinetics (i.e., determination of transition rates).

Although the different precession frequencies at the two environments lead to dephasing of the transverse magnetization (Figure 3c), a 180° radio frequency pulse applied in a transverse direction has the effect of rephasing, and thereby suppressing, exchange-mediated transverse relaxation. This is the essence of a Carr−Purcell−Meiboom−Gill relaxation dispersion (CPMG RD) experiment, where one employs a pulse sequence in which 180° pulses are separated by periods (of duration $2\tau_{cp}$) during which relaxation occurs.[52,53] By varying τ_{cp}, one observes a range of effective transverse relaxation rates ($R_{2,eff}$), and only when $\tau_{cp} \to \infty$ is the effect of chemical exchange fully exhibited. That is, $R_{2,eff}$ is dispersed or spread out as a function of τ_{cp} (or its inverse). In particular, in the fast-exchange regime, $R_{2,eff}$ approaches the value given by eq 10 when $\tau_{cp} \to \infty$ but approaches $\bar{R}_2^0$ when $\tau_{cp} \to 0$. A formula that bridges these two limits of τ_{cp} in the fast exchange regime is[54]

$$R_{2,eff}(\tau_{cp}) = \bar{R}_2^{\,0} + \frac{p_1 p_2 \Delta\omega^2}{k_{ex}}\left[1 - \frac{\tanh(k_{ex}\tau_{cp})}{k_{ex}\tau_{cp}}\right] \tag{11}$$

Fitting the dependence of observed $R_{2,eff}$ on τ_{cp} to eq 11 yields k_{ex} and $p_1 p_2 \Delta\omega^2$.

The conformational exchange that is of practical interest is one between a major state and a minor state (i.e., $p_1 \gg p_2$). A general formula, valid in all three exchange regimes, has been derived for $R_{2,eff}(\tau_{cp})$ of the major state.[55,56] Fitting experimental data can yield the transition rates k_1 and k_2 (and hence the population fraction of the minor state) as well as $\Delta\omega$. The latter is equivalent to the difference in chemical shift between the major and minor states and thus contains structural information about the minor state (chemical shifts in the major state are directly observable). In favorable cases, this information can be used to validate structural models of the minor state.[42] However, the nature of the conformational changes from the major state to the minor state is often poorly defined by CPMG RD experiments, although the millisecond time scale of k_{ex} suggests that the conformational changes must be more than local (Figure 3d).

2.2. Path and Community Analysis

To model protein stability and function in general and allosteric communication in particular, terminologies, ideas, and methods from graph theory[57] have been extensively borrowed and expanded. Typically the protein (composed of N residues) is mapped to a weighted graph, in which each node represents a residue (Figure 4). Two graph properties of interest are the shortest path between two nodes and the partitioning of the graph into communities.

Earlier graph models used the static crystal structure of the protein to specify the weights between nodes. In the simplest version,[58] two nodes were assumed to form an edge and assigned a weight 1 if the distance between two representative atoms of the corresponding residues was within a cutoff; otherwise the weight was 0. (For later reference, the edges in a protein comprise the contact map.) In graph theory,[57] these internode weights define the adjacency matrix:

$$\mathcal{A}_{ij} = 1 \text{ if } i \text{ and } j \text{ are linked by an edge}$$
$$\mathcal{A}_{ij} = 0 \text{ if } i = j \text{ or } i \text{ and } j \text{ are not linked} \tag{12}$$

The sum of the ith row (or column) elements of $\mathcal{A}$ is the degree, that is, the number of edges formed by node i. Denoting the diagonal matrix of degrees as $\mathcal{D}$, the difference

$$\mathcal{L} = \mathcal{D} - \mathcal{A} \tag{13}$$

is known as the Laplacian matrix, which, upon multiplying by a spring constant, happens to coincide with the Hessian matrix of the Gaussian network model[59] (a form of elastic network model). If a value of 1 for the path length of each edge is assumed here, then the total length of a path along connected edges is just the number of edges involved. Any two nodes can

DOI: 10.1021/acs.chemrev.5b00590
Chem. Rev. 2016, 116, 6503−6515

be connected by multiple paths; the shortest paths between residues in the allosteric site and residues in the active site may be especially important for allosteric communication. Atilgan et al.[58] calculated the average of shortest path lengths of a given residue to other residues in a protein and found that average shortest path lengths are highly correlated with amplitudes of residue position thermal fluctuation predicted by the Gaussian network model. Intuitively, hub residues (i.e., those with high degrees) should have both small average shortest path lengths and low amplitudes of thermal fluctuation.

Instead of directly using a cutoff in interresidue distance for specifying edges, Brinda and Vishveshwara[60] used the interresidue interaction strength

$$\mathcal{I}_{ij} = n_{ij}/(n_i n_j)^{1/2} \tag{14}$$

where n_{ij} is the number of atom−atom contacts between residues i and j within a distance cutoff and n_i and n_j are normalization factors. An edge is formed if $\mathcal{I}_{ij}$ exceeds a threshold $\mathcal{I}_{\min}$. (If a molecular dynamics simulation is run, one can further stipulate that an edge is formed only if this condition is satisfied over a specified fraction of the simulation time.[61]) At very high $\mathcal{I}_{\min}$, nodes are disconnected from each other; at very low $\mathcal{I}_{\min}$, all nodes become interconnected; at intermediate $\mathcal{I}_{\min}$, nodes segregate into disconnected communities. A recommended $\mathcal{I}_{\min}$ is one that results in the largest community containing approximately half the residues in the protein.

Chennubhotla and Bahar[62] used eq 14 as the definition of the adjacency matrix. Following graph theory,[57] they assigned the normalized element

$$\mathcal{M}_{ij} = \mathcal{I}_{ij}/\sum_j \mathcal{I}_{ij} \tag{15}$$

as the probability that a random walker through the graph makes a jump from node i to node j. The resulting stationary probabilities of the random walker on the nodes were used to find the probabilities for partitioning each node into different communities. The latter probabilities were further used to define the entropy for partitioning of the node. Nodes with high entropies are shared with high probabilities among multiple communities. These "messenger" nodes may be critical for intercommunity communication in allosteric regulation. For the chaperonin GroEL−GroES complex, these nodes also had small amplitudes in the lowest-frequency mode (i.e., global mode) of the Gaussian network model; the latter occur in hinge regions for interdomain global motions. It remains to be determined whether messenger nodes coincide with another group of residues, also proposed for allosteric communication; the latter residues are identified by a large response in a normal mode of interest when the spring constants for the edges from these residues are perturbed.[63] For path length, rather than a constant value of 1 for each edge, Chennubhotla and Bahar[62] introduced the definition

$$l_{ij} = -\log(\mathcal{M}_{ij}) \tag{16}$$

such that high transition probability corresponds to short path length and vice versa.

Sethi et al.[34] took a major step by using information from molecular dynamics simulations to define the contact map and the path lengths of edges. An edge was formed between two residues, i and j, when the distance between their heavy atoms was below a cutoff for a specified fraction of the simulation time. More importantly, the path lengths of the edges were defined by the (normalized) covariance matrix of the residue positions:

$$l_{ij} = -\log(|C_{ij}|) \tag{17}$$

in analogy to eq 16. The covariance matrix itself is given by

$$C_{ij} = \frac{\langle \mathbf{x}_i \cdot \mathbf{x}_j \rangle}{\langle \mathbf{x}_i \cdot \mathbf{x}_i \rangle^{1/2} \langle \mathbf{x}_i \cdot \mathbf{x}_j \rangle^{1/2}} \tag{18}$$

where $\mathbf{x}_i = \mathbf{r}_i - \langle \mathbf{r}_i \rangle$ are displacements from mean residue positions. When residues i and j are highly correlated in displacement from their mean positions, $|C_{ij}| \to 1$ and, according to eq 17, the path length $l_{ij} \to 0$. Conversely, when the two residues have totally uncorrelated displacements, $|C_{ij}| \to 0$ and $l_{ij} \to \infty$. The total length of a path along connected edges is the sum of the path lengths of the individual edges (Figure 4a); the shortest path between nodes i and j is the path that has the minimum total length among all possible paths connecting i and j.[64]

Sethi et al.[34] used the Girvan−Newman algorithm[65] to partition the graph into communities, within which edges are dense but between which edges are sparse (Figure 4b). The Girvan−Newman algorithm uses edge betweenness, defined as the number of shortest paths that cross a particular edge, for partitioning. The betweenness of an intercommunity edge is high because all the intercommunity shortest paths must cross it (or any small number of other such edges). In contrast, the betweenness of an intracommunity edge is low because many other neighboring edges can provide alternatives for shortest paths. The Girvan−Newman algorithm is an iterative procedure, in which the edge with the highest betweenness is cut and the betweennesses of the remaining edges are recalculated, until every node becomes isolated and hence a community of its own. The partitioning finally chosen is the one with optimal modularity, where the fraction of intracommunity edges maximally exceeds the expected value if the edges are randomly placed between nodes in the graph. Nodes linked by intercommunity edges are termed critical, since all the intercommunity shortest paths cross these edges (Figure 4b). Critical nodes serve a similar role as the messenger nodes of Chennubhotla and Bahar.[62]

Rivalta et al.[66] took the approach of Sethi et al.[34] but redefined the edge path lengths in terms of a generalized correlation matrix introduced by Lange and Grubmuller,[67]

$$C_{ij}^{\mathrm{MI}} = (1 - e^{-2\mathcal{J}_{ij}/3})^{-1/2} \tag{19}$$

where $\mathcal{J}_{ij}$ are the mutual information. The latter,

$$\mathcal{J}_{ij} = \int p(\mathbf{x}_i, \mathbf{x}_j) \ln \frac{p(\mathbf{x}_i, \mathbf{x}_j)}{p_i(\mathbf{x}_i) p_j(\mathbf{x}_j)} \, d\mathbf{x}_i \, d\mathbf{x}_j \tag{20}$$

measures the deviation of the joint probability density $p(\mathbf{x}_i,\mathbf{x}_j)$ of displacements $\mathbf{x}_i$ and $\mathbf{x}_j$ from the product $p_i(\mathbf{x}_i)p_j(\mathbf{x}_j)$ of the two marginal probabilities, which is the expected probability density if $\mathbf{x}_i$ and $\mathbf{x}_j$ are totally uncorrelated. C_{ij}^{MI} reduces to C_{ij} if $p(\mathbf{x}_i,\mathbf{x}_j)$ is Gaussian. When $\mathbf{x}_i$ and $\mathbf{x}_j$ are perpendicular, $C_{ij} = 0$ even if the displacements are highly correlated. This correlation is captured by C_{ij}^{MI}.

DOI: 10.1021/acs.chemrev.5b00590
Chem. Rev. 2016, 116, 6503−6515

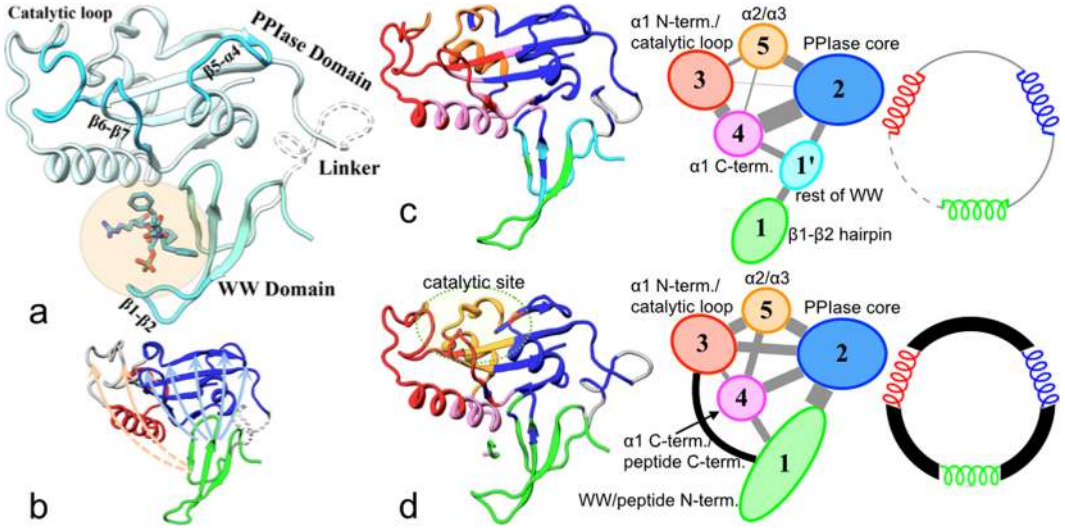

Figure 5. Structure and allosteric communication of Pin1. (a) Structure of Pin1 with FFpSPR bound at the WW site. The catalytic site of the PPIase domain is lined by the three loops labeled as catalytic loop, β5-α4, and β6-β7. (b) Two clusters of paths connecting the WW domain to the catalytic-site loops. The cluster shown as light blue arrows preexists in apo Pin1, but the paths in the second cluster, shown as pink arrows, are broken in the apo form and are completed only in the FFpSPR-bound form. (c,d) Community analysis results for apo and FFpSPR-bound Pin1. The communities are shown in different colors as cartoon structures (left) or as ovals (middle). Intercommunity connections are shown as lines, with width proportional to the cumulative betweenness of intercommunity edges (middle). (Right) Dynamic model for allostery. A spring depicts a representative internal coordinate from each of communities 1, 2, and 3 that is modeled as undergoing diffusive motion in a harmonic potential. The internal coordinates are weakly coupled in apo Pin1 and become strongly coupled in the FFpSPR-bound form.

We remark that the covariance matrix and its generalization measure residue−residue positional correlation during equilibrium fluctuation. Mutual information, expressed in terms of a probability density in conformational space, can be easily recognized as an equilibrium property. The covariance matrix is similarly an equilibrium property, not a dynamic property, even though sometimes it is referred to as the dynamic cross-correlation matrix. Calculation of C_{ij} from molecular dynamics trajectories, by averaging over snapshots, may give it a dynamic appearance, but the time sequence of the snapshots has no effect: the result is the same if the snapshots are scrambled.

Likewise, even though path and community analysis based on residue−residue positional correlation is referred to as dynamical network analysis,[32,34,66,68] strictly speaking, no dynamical information is involved. Given that molecular dynamics simulations used to prepare for path and community analysis typically are submicrosecond in length, and therefore cannot sample microsecond−millisecond conformational exchanges, the information supplied is only quasi-equilibrium. That is, the average is limited to a single conformational state (or a substate therein; Figure 3d).

It is of interest to note that exchange between conformational states has recently been investigated by building Markov state models from molecular dynamics simulations.[30,31,69] In these models, microstates are obtained by clustering snapshots according to structural similarity, and transition probabilities between microstates are estimated from molecular dynamics trajectories.

3. CASE STUDIES OF DYNAMIC EFFECTS IN ALLOSTERIC REGULATION

As noted in the preceding section, allosteric communication is generally thought to be mediated by groups of residues that exhibit effector-induced changes in conformational dynamics or positional correlations. The two types of residues can be identified by NMR spectroscopy and molecular dynamics simulation, respectively. Information from the two approaches can be combined to develop allosteric mechanisms, as illustrated below.

3.1. Pin1

Pin1 is a peptidyl−prolyl cis/trans isomerase (PPIase) that acts on phosphoSer/Thr-Pro [p(S/T)P] motifs present in mitotic phosphoproteins,[70] thereby controlling their fates.[71] The full-length Pin1 consists of an N-terminal WW domain (residues 1−39) and the C-terminal PPIase domain (residues 50−163) (Figure 5a). Both domains can selectively bind p(S/T)P-containing substrate motifs, but only the PPIase domain can isomerize the peptidyl−prolyl bond,[72,73] at a catalytic site lined by three loops (labeled as catalytic loop, β5-α4, and β6-β7 in Figure 5a). In addition to other roles, several lines of evidence suggest that substrate−WW binding allosterically regulates the PPIase activity. First, the substrate affinity and catalytic activity of the isolated PPIase domain are different from those of the full-length protein.[26,72,73] Second, crystal structures of Pin1 show that the two domains are tightly packed against each other, although the linker between them is disordered (Figure 5a).[74−76] Third, NMR studies showed that binding of both substrates and a nonpeptidic ligand [poly(ethylene glycol)] to the WW domain resulted in tighter coupling between the two domains.[77,78] The allosteric communication in Pin1 has been investigated in recent studies based on NMR spectroscopy[26,79−81] and molecular dynamics simulations.[37,82]

Namanja et al.[26,79] obtained the order parameters ($\mathcal{S}^2_{axis}$) for methyl symmetry axes from measurements of methyl ^{2}D relaxation rates. They found that binding of two substrates, one with sequence FFpSPR and the other a pTP-containing peptide from the mitotic phosphatase Cdc25C, both resulted in increases in $\mathcal{S}^2_{axis}$ in three regions (Figure 5b): WW−PPIase interface, interface of α1 helix with PPIase core, and catalytic site. Namanja et al. proposed that these residues, with

DOI: 10.1021/acs.chemrev.5b00590
Chem. Rev. 2016, 116, 6503−6515

suppressed subnanosecond methyl orientational dynamics, formed a hydrophobic conduit for interdomain allosteric regulation. Other methyls also exhibited compensatory decreases in $\mathcal{S}^2_{axis}$ upon peptide binding, with unknown functional implications; more such methyls were found in Cdc25C-bound Pin1 than in FFpSPR-bound Pin1. It should be noted that less than a third of Pin1 residues contain methyls.

To gain a sense of the effect of peptide binding on microsecond-millisecond dynamics, Namanja et al.[26,79] measured methyl ^{13}C longitudinal and transverse relaxation rates and looked for residues with high values for their product, $R_{1;}{}^{13}{}_{C}R_{2;}{}^{13}{}_{C}$, which may indicate contributions from conformational exchange. Upon FFpSPR binding, the number of residues exhibiting $R_{1;}{}^{13}{}_{C}R_{2;}{}^{13}{}_{C}$ increases was more than that for decreases,[83] implicating enhancement of exchange dynamics. Residues with increased $R_{1;}{}^{13}{}_{C}R_{2;}{}^{13}{}_{C}$ map to the WW−PPIase interface and to the interface of α1 and α2 helices with the PPIase core. However, the nature of the minor state with which the major state exchanges remains elusive, if the elevated $R_{1;}{}^{13}{}_{C}R_{2;}{}^{13}{}_{C}$ indeed reflects conformational exchange. For Cdc25C, the trend in $R_{1;}{}^{13}{}_{C}R_{2;}{}^{13}{}_{C}$ changes was apparently reversed, with more decreases than increases. Recent CPMD RD data provided validation of reduced exchange dynamics upon binding Cdc25C and were interpreted as reflecting weakened interdomain contact.[81]

To gain detailed insight into allosteric communication in Pin1, we carried out molecular dynamics simulations of Pin1 in apo form as well as bound with several peptides, either at the WW site or the catalytic site or both sites.[37,82] In the 100 ns simulations, FFpSPR binding at the WW site resulted in decreases in root-mean-square fluctuation (RMSF), indicating suppression of subnanosecond local dynamics, in the three loops lining the catalytic site, to the level exhibited when a trans-locked alkene isostere of FFpSPR was bound to both WW and catalytic sites. The FFpSPR-induced reduction in RMSF for the catalytic-site loops is a clear indication of allosteric communication between the two binding sites. The communication evidently was unidirectional, as a cis-locked alkene isostere bound only at the catalytic site did not produce loss in flexibility in the WW domain.

We used the graph-partitioning method of Brinda and Vishveshwara,[60] which is based on residue−residue physical proximity, to identify allosteric pathways. The partitioning produced two clusters of paths for FFpSPR-bound Pin1. The first emanates from the WW backside and propagates through the interdomain interface and the PPIase domain core to the β5-α4 and β6-β7 loops; the second emanates from the WW front pocket and propagates through the bound peptide, the α1 helix, and the latter's interface with the PPIase core to the catalytic loop. The first cluster of paths preexists in apo Pin1, but the second cluster is broken as the gap between the α1 helix and the WW front pocket is too wide without the bound peptide (Figure 5b). In essence, the bound peptide serves as a bridge to complete the second cluster of paths from the WW site to the catalytic site.

We also applied the community analysis method of Sethi et al.,[34] which is based on both physical proximity and positional correlation. The overall conclusion was the same, but new insight emerged. The WW front pocket, β5-α4 loop, and β6-β7 and catalytic loops are located in three different communities (numbered 1, 2, and 3, respectively, in Figure 5c,d, left and middle). In apo Pin1, community 1 is not directly linked to either community 2 or 3. In FFpSPR-bound Pin1, community 1 is enlarged to include the whole WW domain and the N-terminal region of the peptide. It is now directly linked to community 3, with the N-terminal residues of the peptide providing critical nodes for linkage. Moreover, the enlarged community 1 becomes directly and strongly linked to community 2. The strengthened coupling between these communities thus explains the allosteric communication.

The foregoing analyses suggested that FFpSPR elicits allosteric effects by serving as a bridge to connect the α1 helix and the WW domain. To test this idea, we carried out simulations in which subsets of residues in different regions of apo Pin1 were artificially restrained to limit conformational fluctuations and monitored the RMSF of catalytic-site loops. The RMSF was hardly changed with restraint of the WW domain or within the PPIase core, and only partially reduced with restraint of the PPIase core and α1 helix interface, but RMSF was fully reduced when four residues from the WW domain were added into the restraint. Importantly, the reference conformation in these restraints was taken from the simulation of apo Pin1. So these restrained simulations directly demonstrated the idea[4] that merely restricting the fluctuations around a mean structure can generate allosteric effects, while also showing that restrictions in different regions of a protein are not equally effective.

Our followup study[82] showed that, compared to FFpSPR, Cdc25C more tightly interacted with the WW domain but less so with the α1 helix and the PPIase core. As a result, community 1 lost direct linkage to communities 2 and 3 (as in apo Pin1), and the suppression of subnanosecond local dynamics (as indicated by RMSF) was not as effective, in line with NMR studies.[26,79] NMR[80] and molecular dynamics simulation[37] studies of the I28A mutant, within the WW−PPIase interface, provided additional evidence that weakened intercommunity coupling leads to reduced suppression of subnanosecond local dynamics. Note that when the cis-locked alkene isostere is bound at the PPIase catalytic site, the bridge between the α1 helix and the WW domain is missing, and hence communication from PPIase to WW domain is ineffective. This provides a simple explanation for the apparent unidirectionality of allosteric communication between WW and catalytic sites.

Why should the amplitude of subnanosecond local dynamics be related to intercommunity coupling, which is based on physical proximity and positional correlation? To illustrate this point, let us consider the local dynamics of the unit vector **n**, shown in Figure 3a,b, in two extremes. In one extreme, local dynamics is fully quenched, with the unit vector rigidly attached to the protein so that the order parameter $\mathcal{S}^2$ is 1. Of course this unit vector would be fully correlated with any other such unit vector since they both follow the same overall tumbling of the protein. The correlation time of **n** is that of overall tumbling, that is, τ_c, which is on the order of 10 ns. In the other extreme, the local dynamics completely randomizes the orientation of **n**, resulting in $\mathcal{S}^2 = 0$. Obviously **n** would be totally uncorrelated with any other such unit vector. Now the correlation time of **n** (see eq 5 with $\mathcal{S}^2 = 0$) is $\tau_c\tau_e/(\tau_c + \tau_e) \approx \tau_e$, since $\tau_c \gg \tau_e$, which is subnanosecond. So in this example, increased intercommunity coupling is correlated with quenching of fast, subnanosecond dynamics and emergence of slower, 10 ns dynamics.

DOI: 10.1021/acs.chemrev.5b00590
Chem. Rev. 2016, 116, 6503−6515

To further explore the relationship between intercommunity coupling and dynamics on fast and slow time scales, we introduced a dynamic model of allostery (Figure 5c,d, right). This model was inspired by the molecular dynamics simulation and community analysis results for Pin1 summarized above (Figure 5c,d, left and middle) but highly simplified. We modeled a representative internal coordinate from each of communities 1, 2, and 3 as undergoing diffusive motion in a harmonic potential. The strength of coupling between the internal coordinates was tunable, from very weak for apo Pin1 to very strong for the FFpSPR-bound form. This model predicts that, with weak coupling, the internal coordinates have a single-exponential time-correlation function with a short correlation time (e.g., subnanosecond). However, with strong coupling, the time-correlation function is a double exponential; one exponential has a short correlation time and a small amplitude, while the second exponential has a long correlation time (e.g., microsecond−millisecond) and a large amplitude. That is, with increasing intercommunity coupling, the fast motion is suppressed and replaced by slow motion. Internal coordinates from the different communities also become highly correlated. The slow motion may represent conformational exchange, insofar as the latter requires intercommunity correlated motions (Figure 3d).

Our model suggests that, with strengthened intercommunity coupling, suppression of fast local dynamics may be expected along with initiation of slow conformational exchange dynamics. The NMR results summarized above provide some support. With FFpSPR, $\mathcal{S}^2_{\text{axis}}$ data indicated suppression of local dynamics, whereas $R_{1;^{13}\text{C}}R_{2;^{13}\text{C}}$ data indicated enhanced conformational exchange. With Cdc25C, both effects were moderated. It appears that allosteric activators like FFpSPR, by strengthening intercommunity coupling, in particular through providing critical nodes, may elicit disparate dynamic responses on fast and slow time scales.

3.2. Imidazole Glycerol Phosphate Synthase

Imidazole glycerol phosphate synthase (IGPS) is a bifunctional enzyme with active sites located in two separate domains named HisH and HisF (which are associated noncovalently in bacteria but are covalently linked in eukaryotes; Figure 6). HisH catalyzes the hydrolysis of glutamine into glutamate and ammonia, using a conserved catalytic triad consisting of Cys84, His178, and Glu180 (*Thermotoga maritima* IGPS numbering), located ∼10 Å away from the HisH−HisF interface. This reaction starts with thioester bond formation between glutamine and Cys84, with the resulting oxyanion tetrahedral intermediate stabilized by the backbone amide of Val51, part of a conserved PGVG motif. The ammonia product then travels down a 20 Å hydrophobic tunnel formed by the β strands of the HisF $(\beta/\alpha)_8$ barrel to the second active site at the bottom, where it combines with metabolite *N*′-[(5′ -phosphoribulosyl)-formimino]-5-aminoimidazole-4-carboxamide ribonucleotide (PRFAR) to yield two products that enter the histidine and purine biosynthetic pathways. Coordination of the two reactions is achieved through PRFAR serving as an allosteric effector. Binding of PRFAR to the HisF active site enhances the k_{cat} of HisH by ∼5000-fold.[84] The long PRFAR molecule, with the two ends near residues Val100 and Leu222, respectively, bisects the bottom of the HisF $(\beta/\alpha)_8$ barrel with $\beta1/\alpha1$, $\beta2/\alpha2$, and $\beta3/\alpha3$ on one side and $\beta5/\alpha5$, $\beta6/\alpha6$, and $\beta7/\alpha7$ on the other side (referred to as side R and side L, respectively).[66] The allosteric effects of PRFAR binding were studied by both

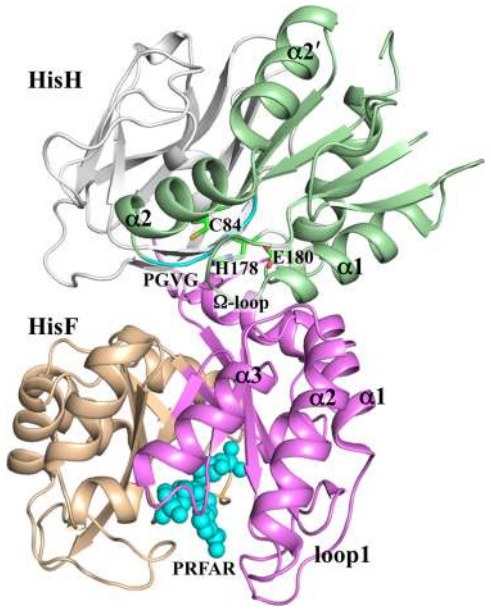

Figure 6. Structure of IGPS. Side L and side R are shown in light orange and magenta, respectively, for HisF and in gray and green, respectively for HisH. HisF side L consists of residues 101−220, and HisH side R consists of $\beta1$−$\beta4$ strands, $\alpha1$, $\alpha2$, $\alpha2'$, and $\alpha4$ helices, and Ω-loop. The bound PRFAR in HisF is shown as cyan spheres, and the catalytic triad and PGVG motif are labeled, as are some secondary structure elements ($\alpha1$−$\alpha3$ and loop1 in HisF and $\alpha1$, $\alpha2$, $\alpha2'$, and Ω-loop in HisH).

NMR spectroscopy and molecular dynamics simulations.[28,40,66,68]

From CPMG RD experiments on backbone ^{15}N and alanine methyl ^{13}C, Lipchock et al.[40] found no evidence of HisF exchange dynamics in apo IGPS. Methyl-^{13}C RD data on isoleucines, leucines, and valines (ILV) showed signs of conformational exchange for 17 of 116 assigned resonances from HisF, mostly on side R. Upon PRFAR binding, 63 backbone amide resonances from HisF were broadened beyond detection, indicative of the intermediate exchange regime, mostly on side R. Backbone ^{15}N and ILV methyl-^{13}C RD data together identified 68 HisF residues as undergoing millisecond conformational exchange, and the active ILV residues spread to the entire central β barrel and the β/α interface. On the other hand, ^{1}H−^{1}H dipolar cross-correlated relaxation rates of HisF ILV residues did not indicate a significant overall change in subnanosecond dynamics upon PRFAR binding. It was unknown whether PRFAR had any effect on fast dynamics of other side chains or the protein backbone.

In the crystal structure of apo IGPS, the peptide plane between Gly50 and Val51 of HisH is in an orientation opposite to what would provide stabilization to the oxyanion tetrahedral intermediate, with the Gly50 carbonyl oxygen instead of the Val51 amide proton pointing to the negatively charged oxygen atom of the would-be tetrahedral intermediate.[85] The Val51 amide instead hydrogen-bonds to the carbonyl of Pro10. The ^{1}H,^{15}N NMR spectrum of Lipchock et al.[40] for HisH in apo IGPS showed a sharp cross peak for Gly50, which was broadened beyond detection upon titration with PRFAR. This observation showed that PRFAR-stimulated millisecond exchange dynamics extended across the HisF−HisH interface and into the active site of HisH. Lipchock et al.[40] proposed that this exchange dynamics allowed the Gly50−Val51 peptide

DOI: 10.1021/acs.chemrev.5b00590
Chem. Rev. 2016, 116, 6503−6515

plane to flip and thus present the stabilizing amide proton of Val51.

Rivalta et al.[66] reported 100 ns molecular dynamics simulations of apo and PRFAR-bound IGPS. PRFAR binding resulted in an overall decrease in RMSF in HisF, especially its loop 1 (residues 16−30), but not in HisH. The decrease in RMSF means that the amplitudes of local subnanosecond dynamics were suppressed. The PRFAR-induced changes in positional correlation, as captured by the generalized correlation matrix calculated from mutual information, were heterogeneous. Positional correlations were reduced in HisF side L (residues 101−220) and in the HisH catalytic triad and surrounding residues, including the PGVG motif. However, correlations were enhanced within and between HisF side R (including loop1, α2 and α3 helices, and β3 strand) and HisH elements on the same side (including β1−β3 strands, α1 helix, and intervening Ω-loop) (Figure 6).

Using the generalized correlation matrix to define edge pass lengths, Rivalta et al.[66] carried out community analysis. One of the most notable changes induced by PRFAR binding was the strengthened coupling between a community in HisF and a community in HisH, both on side R (Figure 6). The HisF community included β2/β3 strands and α2/α3 helices; the HisH community included β1−β4 strands, α1, α2, α2′, and α4 helices, and Ω-loop. The two communities were linked by edges between residues in HisF α2/α3 helices and in HisH α1 helix and Ω-loop. The strengthened intercommunity coupling was in line with the increased positional correlations between these elements.

In these molecular dynamics simulations, the HisH Val51−Pro10 hydrogen bond was stable in apo IGPS but unstable in the PRFAR-bound form. Concomitantly, the Gly50−Val51 peptide plane partially rotated, which the authors suggested as an early sign of an anticipated full flip of the peptide plane in the millisecond time scale.

The foregoing NMR and computational results appear to be qualitatively consistent with the predictions of our simple dynamic model of allostery (Figure 5c,d, right). That is, upon PRFAR binding, the coupling between two communities across the interdomain interface was strengthened, while the amplitudes of subnanosecond local dynamics were suppressed (as indicated by reduced RMSF) and millisecond exchange dynamics was stimulated (as revealed by NMR spectroscopy). However, instead of the disparate responses of fast and slow dynamics that we emphasize, Rivalta et al.[28,66] appear to suggest that fast and slow dynamics go hand in hand. According to them, disruptions of residue−residue interactions on the nanosecond time scale "may represent the initial loosening of the protein core that precedes the wholesale enhancement of ms motions observed by solution NMR." Clearly, the nature of millisecond exchange dynamics, although beyond the scope of submicrosecond molecular dynamics simulations, deserves further studies.

Vanwart et al.[68] also carried out molecular dynamics simulations and community analysis for apo and PRFAR-bound IGPS. Their focus was how different representatives of residues positions, for example, Cα atom versus residue center of mass, affected community partitioning. The latter representative was recommended.

4. PERSPECTIVES

We have assessed the potential roles of conformational dynamics in the allosteric regulation of two proteins. From NMR spectroscopy, a hydrophobic conduit was proposed for interdomain communication in Pin1, based on suppressed side-chain subnanosecond dynamics upon effector binding;[26,79] effector-stimulated millisecond conformational exchange dynamics was proposed to allow for a peptide plane flip anticipated for IGPS activation.[40] From molecular dynamics simulation and community analysis, effector binding was found to strengthen the coupling between communities across the interdomain interfaces in both Pin1[37,82] and IGPS.[66] It is clear that characterizing the conformational dynamics in these proteins has led to better understanding of their allosteric regulation. It is also clear that NMR spectroscopy and molecular dynamics simulation are highly complementary in developing allosteric mechanisms.

Much remains to be learned. One contentious issue is the relationship between fast local dynamics and slow conformational exchange dynamics. One view is that stimulation of the slow dynamics may be accompanied by suppression of the fast dynamics, both of which are related to strengthening of intercommunity coupling.[82] An opposite view is that disruptions of residue−residue interactions, mediated by strong fast dynamics, may precedes enhancement of slow exchange dynamics. One can fault the first view for the simplicity of the theoretical model used to predict it and the second view for making inference across 6 orders of magnitude in time. It might be possible to settle this issue through theoretical models that have more molecular ingredients.

Many workers have invoked the term allosteric signal. If there is such a signal, can one experimentally measure its speed of propagation? A recent experiment on a ligand-gated ion channel has the appearance of such a measurement, in which a brief application of an agonist was followed by single-channel recordings of currents through the transmembrane channel.[86] The delayed response in currents might be construed as indicating the time needed for propagating an allosteric signal from the ligand-binding domain to the transmembrane channel. However, following the common practice in single-channel electrophysiology, the current response was fit to a kinetic model, with rate constants for agonist binding and unbinding and for conformational transitions of the multidomain channel protein (including opening and closing of the transmembrane channel). It certainly is more insightful to interpret the delay in current response as due to events including agonist binding and channel closed-to-open transition than as due to the propagation of some allosteric signal. Pump−probe molecular dynamics simulations, in which selected atoms are pumped by oscillating forces,[87] and time-resolved femtosecond crystallography enabled by X-ray free electron lasers[88,89] might be able to shed light on issues surrounding allosteric signal.

From the apo form to the ternary complex, the same free energy change is accumulated whether effector binding is followed by substrate binding or vice versa. Accordingly, the change in free energy for substrate binding by the prebinding of an effector is the same as the change in free energy of effector binding by prebinding of the substrate (both equal to the free energy of cooperation). This thermodynamic reciprocity implies that allosteric communication is always bidirectional. Our molecular dynamics simulations evidently showed unidirectional allosteric communication in Pin1: while substrate binding to the WW domain resulted in suppression of local dynamics in the PPIase catalytic-site loops, substrate binding to the PPIase did not produce suppression of the local dynamics in the WW domain. Note that this unidirectionality does not

DOI: 10.1021/acs.chemrev.5b00590
Chem. Rev. 2016, 116, 6503−6515

violate thermodynamic reciprocity because the former concerns only the events of binding a single ligand (at either the WW or catalytic site), whereas the latter involves simultaneous occupation of both sites. This unidirectionality in Pin1 comes about because the WW-bound substrate serves as a bridge to strengthen interdomain communication, whereas this bridge is missing when the substrate is bound to the PPIase. Unidirectional allosteric communication was also seen in molecular dynamics simulations of sortase A, where allosteric activation appears to be mediated by the disorder-to-order transition of a long loop.[90] Yet another example was revealed by NMR spectroscopy for communication between the two cAMP binding sites (named A and B) in the RIα subunit of protein kinase A.[91,92] Upon site A binding, spectral changes spread to the whole protein, but upon site B binding, spectral changes were confined to the B domain only. Examples like these can serve as important test cases for validating ideas about allosteric communication.

Are allosteric proteins endowed with special structural, energetic, or dynamic properties, or can any protein potentially be allosteric? The latter view, argued by Gunasekaran et al.,[93] seems to have support. For example, dynamic and conformational changes in response to Val to Ala mutations in a small protein, eglin c, previously not known to be allosteric, were detected at sites as far as 16 Å away.[94] Moreover, screening with compound libraries identified secondary binding sites on many proteins, and binding of small molecules to these newly identified sites modulated protein functions.[95] On the other hand, not all dynamic and conformational changes in an allosteric protein are equal in mediating allosteric communication. It is important to design control systems to validate proposed mechanisms of allosteric communication.

Such validation can be very effectively done by designed molecular dynamics simulations. Our simulations with artificial restraints on Pin1 offered a glimpse into the potential of this approach. To make our idea about the critical importance of the α1−WW bridge experimentally testable, we introduced an α1−WW cross-link, and our molecular dynamics simulations of this construct indeed showed suppression of fast dynamics for the catalytic-site loops, similar to the effect induced by substrate−WW binding.[82] This predicted effect on fast dynamics awaits experimental test. On another front, a method called accelerated molecular dynamics, designed to artificially reduce free energy barriers, has already met with success in exploring the roles of microsecond−millisecond time-scale dynamics in allosteric communication.[43]

While this review has focused on structured proteins, allostery in intrinsically disordered proteins and proteins with intrinsically disordered regions is emerging as an exciting frontier.[90,96,97] Conformational dynamics in these proteins can be anticipated to play even greater roles in allosteric communication, although they are only starting to be appreciated.[90]

AUTHOR INFORMATION

Corresponding Author

*E-mail hzhou4@fsu.edu.

Notes

The authors declare no competing financial interest.

Biographies

Jingjing Guo received her Ph.D. in medicinal chemistry from Lanzhou University (China) in 2015 under the supervision of Professor Huanxiang Liu. From 2013 to 2015, she studied as a visiting student with Professor Huan-Xiang Zhou at Florida State University, conducting research on protein allostery. She is now a lecturer at Henan Normal University (China).

Huan-Xiang Zhou received his Ph.D. from Drexel University in 1988. He did postdoctoral work at the National Institutes of Health with Attila Szabo. After faculty appointments at Hong Kong University of Science and Technology and Drexel, he moved in 2002 to Florida State University, where he is now Distinguished Research Professor. He has served on a number of grant review panels and journal editorial boards. His group currently does theoretical, computational, and experimental research on protein association, on crowding and emergent properties of cellular environments, on structures and functional mechanisms of ion channels and other membrane proteins, and on self-assembly of peptides.

ACKNOWLEDGMENTS

This work was supported by Grant GM0585187 from the National Institutes of Health.

REFERENCES

(1) Monod, J.; Jacob, F. General Conclusions: Telenomic Mechanisms in Cellular Metabolism, Growth, and Differentiation. *Cold Spring Harbor Symp. Quant. Biol.* **1961**, *26*, 389−401.
(2) Monod, J.; Wyman, J.; Changeux, J.-P. On the Nature of Allosteric Transitions: A Plausible Model. *J. Mol. Biol.* **1965**, *12*, 88−118.
(3) Wyman, J.; Allen, D. W. The Problem of the Heme Interactions in Hemoglobin and the Basis of the Bohr Effect. *J. Polym. Sci.* **1951**, *7*, 499−518.
(4) Cooper, A.; Dryden, D. T. Allostery without Conformational Change. A Plausible Model. *Eur. Biophys. J.* **1984**, *11*, 103−109.
(5) Nussinov, R.; Tsai, C. J. Allostery without a Conformational Change? Revisiting the Paradigm. *Curr. Opin. Struct. Biol.* **2015**, *30*, 17−24.
(6) Dai, J.; Zhou, H. X. Reduced Curvature of Ligand-Binding Domain Free-Energy Surface Underlies Partial Agonism at NMDA Receptors. *Structure* **2015**, *23*, 228−236.
(7) Dai, J.; Wollmuth, L. P.; Zhou, H. X. Mechanism-Based Mathematical Model for Gating of Ionotropic Glutamate Receptors. *J. Phys. Chem. B* **2015**, *119*, 10934−10940.
(8) Koshland, D. E. Application of a Theory of Enzyme Specificity to Protein Synthesis. *Proc. Natl. Acad. Sci. U.S.A.* **1958**, *44*, 98−104.
(9) Burgen, A. S. Conformational Changes and Drug Action. *Fed. Proc.* **1981**, *40*, 2723−2728.
(10) Ma, B.; Kumar, S.; Tsai, C. J.; Nussinov, R. Folding Funnels and Binding Mechanisms. *Protein Eng., Des. Sel.* **1999**, *12*, 713−720.
(11) Formaneck, M. S.; Ma, L.; Cui, Q. Reconciling the "Old" and "New" Views of Protein Allostery: A Molecular Simulation Study of Chemotaxis Y Protein (Chey). *Proteins: Struct., Funct., Genet.* **2006**, *63*, 846−867.
(12) Boehr, D. D.; Nussinov, R.; Wright, P. E. The Role of Dynamic Conformational Ensembles in Biomolecular Recognition. *Nat. Chem. Biol.* **2009**, *5*, 789−796.
(13) Koshland, D. E., Jr.; Nemethy, G.; Filmer, D. Comparison of Experimental Binding Data and Theoretical Models in Proteins Containing Subunits. *Biochemistry* **1966**, *5*, 365−385.
(14) Greives, N.; Zhou, H. X. Both Protein Dynamics and Ligand Concentration Can Shift the Binding Mechanism between Conformational Selection and Induced Fit. *Proc. Natl. Acad. Sci. U.S.A.* **2014**, *111*, 10197−10202.

DOI: 10.1021/acs.chemrev.5b00590
Chem. Rev. 2016, 116, 6503−6515

(15) Hammes, G. G.; Wu, C. W. Kinetics of Allosteric Enzymes. *Annu. Rev. Biophys. Bioeng.* **1974**, *3*, 1−33.
(16) Hammes, G. G.; Chang, Y. C.; Oas, T. G. Conformational Selection or Induced Fit: A Flux Description of Reaction Mechanism. *Proc. Natl. Acad. Sci. U.S.A.* **2009**, *106*, 13737−13741.
(17) Zhou, H.-X. From Induced Fit to Conformational Selection: A Continuum of Binding Mechanism Controlled by the Timescale of Conformational Transitions. *Biophys. J.* **2010**, *98*, L15−L17.
(18) Perutz, M. F. Stereochemistry of Cooperative Effects in Haemoglobin. *Nature* **1970**, *228*, 726−739.
(19) Eaton, W. A.; Henry, E. R.; Hofrichter, J.; Bettati, S.; Viappiani, C.; Mozzarelli, A. Evolution of Allosteric Models for Hemoglobin. *IUBMB Life* **2007**, *59*, 586−599.
(20) Cui, Q.; Karplus, M. Allostery and Cooperativity Revisited. *Protein Sci.* **2008**, *17*, 1295−1307.
(21) Wrabl, J. O.; Gu, J.; Liu, T.; Schrank, T. P.; Whitten, S. T.; Hilser, V. J. The Role of Protein Conformational Fluctuations in Allostery, Function, and Evolution. *Biophys. Chem.* **2011**, *159*, 129−141.
(22) Volkman, B. F.; Lipson, D.; Wemmer, D. E.; Kern, D. Two-State Allosteric Behavior in a Single-Domain Signaling Protein. *Science* **2001**, *291*, 2429−2433.
(23) Yan, J.; Liu, Y.; Lukasik, S. M.; Speck, N. A.; Bushweller, J. H. CBFbeta Allosterically Regulates the Runx1 Runt Domain Via a Dynamic Conformational Equilibrium. *Nat. Struct. Mol. Biol.* **2004**, *11*, 901−906.
(24) Popovych, N.; Sun, S.; Ebright, R. H.; Kalodimos, C. G. Dynamically Driven Protein Allostery. *Nat. Struct. Mol. Biol.* **2006**, *13*, 831−838.
(25) Petit, C. M.; Zhang, J.; Sapienza, P. J.; Fuentes, E. J.; Lee, A. L. Hidden Dynamic Allostery in a PDZ Domain. *Proc. Natl. Acad. Sci. U.S.A.* **2009**, *106*, 18249−18254.
(26) Namanja, A. T.; Wang, X. J.; Xu, B.; Mercedes-Camacho, A. Y.; Wilson, K. A.; Etzkorn, F. A.; Peng, J. W. Stereospecific Gating of Functional Motions in Pin1. *Proc. Natl. Acad. Sci. U.S.A.* **2011**, *108*, 12289−12294.
(27) Ruschak, A. M.; Kay, L. E. Proteasome Allostery as a Population Shift Between Interchanging Conformers. *Proc. Natl. Acad. Sci. U.S.A.* **2012**, *109*, E3454−3462.
(28) Manley, G.; Rivalta, I.; Loria, J. P. Solution NMR and Computational Methods for Understanding Protein Allostery. *J. Phys. Chem. B* **2013**, *117*, 3063−3073.
(29) Dror, R. O.; Green, H. F.; Valant, C.; Borhani, D. W.; Valcourt, J. R.; Pan, A. C.; Arlow, D. H.; Canals, M.; Lane, J. R.; Rahmani, R.; et al. Structural Basis for Modulation of a G-Protein-Coupled Receptor by Allosteric Drugs. *Nature* **2013**, *503*, 295−299.
(30) Malmstrom, R. D.; Kornev, A. P.; Taylor, S. S.; Amaro, R. E. Allostery through the Computational Microscope: cAMP Activation of a Canonical Signalling Domain. *Nat. Commun.* **2015**, *6*, No. 7588.
(31) Pontiggia, F.; Pachov, D. V.; Clarkson, M. W.; Villali, J.; Hagan, M. F.; Pande, V. S.; Kern, D. Free Energy Landscape of Activation in a Signalling Protein at Atomic Resolution. *Nat. Commun.* **2015**, *6*, 7284.
(32) Feher, V. A.; Durrant, J. D.; Van Wart, A. T.; Amaro, R. E. Computational Approaches to Mapping Allosteric Pathways. *Curr. Opin. Struct. Biol.* **2014**, *25*, 98−103.
(33) Suel, G. M.; Lockless, S. W.; Wall, M. A.; Ranganathan, R. Evolutionarily Conserved Networks of Residues Mediate Allosteric Communication in Proteins. *Nat. Struct. Biol.* **2003**, *10*, 59−69.
(34) Sethi, A.; Eargle, J.; Black, A. A.; Luthey-Schulten, Z. Dynamical Networks in tRNA:Protein Complexes. *Proc. Natl. Acad. Sci. U.S.A.* **2009**, *106*, 6620−6625.
(35) Motlagh, H. N.; Wrabl, J. O.; Li, J.; Hilser, V. J. The Ensemble Nature of Allostery. *Nature* **2014**, *508*, 331−339.
(36) Wand, A. J.; Kern, D. On the Dynamic Origins of Allosteric Activation. *Science* **2001**, *293*, 1395.
(37) Guo, J.; Pang, X.; Zhou, H. X. Two Pathways Mediate Interdomain Allosteric Regulation in Pin1. *Structure* **2015**, *23*, 237−247.
(38) Tzeng, S. R.; Kalodimos, C. G. Protein Dynamics and Allostery: An NMR View. *Curr. Opin. Struct. Biol.* **2011**, *21*, 62−67.
(39) Zhuravleva, A.; Gierasch, L. M. Substrate-Binding Domain Conformational Dynamics Mediate Hsp70 Allostery. *Proc. Natl. Acad. Sci. U.S.A.* **2015**, *112*, E2865−2873.
(40) Lipchock, J. M.; Loria, J. P. Nanometer Propagation of Millisecond Motions in V-Type Allostery. *Structure* **2010**, *18*, 1596−1607.
(41) Srivastava, A. K.; McDonald, L. R.; Cembran, A.; Kim, J.; Masterson, L. R.; McClendon, C. L.; Taylor, S. S.; Veglia, G. Synchronous Opening and Closing Motions Are Essential for cAMP-Dependent Protein Kinase a Signaling. *Structure* **2014**, *22*, 1735−1743.
(42) Oyen, D.; Fenwick, R. B.; Stanfield, R. L.; Dyson, H. J.; Wright, P. E. Cofactor-Mediated Conformational Dynamics Promote Product Release from *Escherichia Coli* Dihydrofolate Reductase Via an Allosteric Pathway. *J. Am. Chem. Soc.* **2015**, *137*, 9459−9468.
(43) Gasper, P. M.; Fuglestad, B.; Komives, E. A.; Markwick, P. R.; McCammon, J. A. Allosteric Networks in Thrombin Distinguish Procoagulant vs. Anticoagulant Activities. *Proc. Natl. Acad. Sci. U.S.A.* **2012**, *109*, 21216−21222.
(44) Palmer, A. G., III. NMR Characterization of the Dynamics of Biomacromolecules. *Chem. Rev.* **2004**, *104*, 3623−3640.
(45) Pervushin, K.; Riek, R.; Wider, G.; Wuthrich, K. Attenuated T_2 Relaxation by Mutual Cancellation of Dipole-Dipole Coupling and Chemical Shift Anisotropy Indicates an Avenue to NMR Structures of Very Large Biological Macromolecules in Solution. *Proc. Natl. Acad. Sci. U.S.A.* **1997**, *94*, 12366−12371.
(46) Lipari, G.; Szabo, A. Model-Free Approach to the Interpretation of Nuclear Magnetic Resonance Relaxation in Macromolecules. 1. Theory and Range of Validity. *J. Am. Chem. Soc.* **1982**, *104*, 4546−4559.
(47) Showalter, S. A.; Bruschweiler, R. Validation of Molecular Dynamics Simulations of Biomolecules Using NMR Spin Relaxation as Benchmarks: Application to the Amber99SB Force Field. *J. Chem. Theory Comput.* **2007**, *3*, 961−975.
(48) Maragakis, P.; Lindorff-Larsen, K.; Eastwood, M. P.; Dror, R. O.; Klepeis, J. L.; Arkin, I. T.; Jensen, M. O.; Xu, H. F.; Trbovic, N.; Friesner, R. A.; et al. Microsecond Molecular Dynamics Simulation Shows Effect of Slow Loop Dynamics on Backbone Amide Order Parameters of Proteins. *J. Phys. Chem. B* **2008**, *112*, 6155−6158.
(49) Yang, D.; Kay, L. E. Contributions to Conformational Entropy Arising from Bond Vector Fluctuations Measured from NMR-Derived Order Parameters: Application to Protein Folding. *J. Mol. Biol.* **1996**, *263*, 369−382.
(50) Li, Z.; Raychaudhuri, S.; Wand, A. J. Insights into the Local Residual Entropy of Proteins Provided by NMR Relaxation. *Protein Sci.* **1996**, *5*, 2647−2650.
(51) Wand, A. J. The Dark Energy of Proteins Comes to Light: Conformational Entropy and Its Role in Protein Function Revealed by NMR Relaxation. *Curr. Opin. Struct. Biol.* **2013**, *23*, 75−81.
(52) Carr, H. Y.; Purcell, E. M. Effects of Diffusion on Free Precession in Nuclear Magnetic Resonance Experiments. *Phys. Rev.* **1954**, *94*, 630−638.
(53) Meiboom, S.; Gill, D. Modified Spin-Echo Method for Measuring Nuclear Relaxation Times. *Rev. Sci. Instrum.* **1958**, *29*, 688−691.
(54) Luz, Z.; Meiboom, S. Nuclear Magnetic Resonance Study of Protolysis of Trimethylammonium Ion in Aqueous Solution - Order of Reaction with Respect to Solvent. *J. Chem. Phys.* **1963**, *39*, 366−370.
(55) Carver, J. P.; Richards, R. E. General Two-Site Solution for Chemical Exchange Produced Dependence of T_2 Upon Carr-Purcell Pulse Separation. *J. Magn. Reson.* **1972**, *6*, 89−105.
(56) Baldwin, A. J. An Exact Solution for $R_{2,Eff}$ in CPMG Experiments in the Case of Two Site Chemical Exchange. *J. Magn. Reson.* **2014**, *244*, 114−124.
(57) Chung, F. R. K. *Spectral Graph Theory*; CBMS Regional Conference Series in Mathematics, Number 92; American Mathematical Society Publications, 1997.

DOI: 10.1021/acs.chemrev.5b00590
Chem. Rev. 2016, 116, 6503−6515

(58) Atilgan, A. R.; Akan, P.; Baysal, C. Small-World Communication of Residues and Significance for Protein Dynamics. *Biophys. J.* **2004**, *86*, 85−91.
(59) Bahar, I.; Atilgan, A. R.; Erman, B. Direct Evaluation of Thermal Fluctuations in Proteins Using a Single-Parameter Harmonic Potential. *Folding Des.* **1997**, *2*, 173−181.
(60) Brinda, K. V.; Vishveshwara, S. A Network Representation of Protein Structures: Implications for Protein Stability. *Biophys. J.* **2005**, *89*, 4159−4170.
(61) Seeber, M.; Felline, A.; Raimondi, F.; Muff, S.; Friedman, R.; Rao, F.; Caflisch, A.; Fanelli, F. Wordom: A User-Friendly Program for the Analysis of Molecular Structures, Trajectories, and Free Energy Surfaces. *J. Comput. Chem.* **2011**, *32*, 1183−1194.
(62) Chennubhotla, C.; Bahar, I. Markov Propagation of Allosteric Effects in Biomolecular Systems: Application to Groel-Groes. *Mol. Syst. Biol.* **2006**, *2*, 36.
(63) Zheng, W.; Brooks, B. R.; Thirumalai, D. Allosteric Transitions in the Chaperonin GroEL Are Captured by a Dominant Normal Mode That Is Most Robust to Sequence Variations. *Biophys. J.* **2007**, *93*, 2289−2299.
(64) Floyd, R. W. Algorithm-97 - Shortest Path. *Commun. ACM* **1962**, *5*, 345−345.
(65) Girvan, M.; Newman, M. E. Community Structure in Social and Biological Networks. *Proc. Natl. Acad. Sci. U.S.A.* **2002**, *99*, 7821−7826.
(66) Rivalta, I.; Sultan, M. M.; Lee, N. S.; Manley, G. A.; Loria, J. P.; Batista, V. S. Allosteric Pathways in Imidazole Glycerol Phosphate Synthase. *Proc. Natl. Acad. Sci. U.S.A.* **2012**, *109*, E1428−1436.
(67) Lange, O. F.; Grubmuller, H. Generalized Correlation for Biomolecular Dynamics. *Proteins: Struct., Funct., Genet.* **2006**, *62*, 1053−1061.
(68) Vanwart, A. T.; Eargle, J.; Luthey-Schulten, Z.; Amaro, R. E. Exploring Residue Component Contributions to Dynamical Network Models of Allostery. *J. Chem. Theory Comput.* **2012**, *8*, 2949−2961.
(69) Vanatta, D. K.; Shukla, D.; Lawrenz, M.; Pande, V. S. A Network of Molecular Switches Controls the Activation of the Two-Component Response Regulator NtrC. *Nat. Commun.* **2015**, *6*, 7283.
(70) Lu, K. P.; Hanes, S. D.; Hunter, T. A Human Peptidyl−Prolyl Isomerase Essential for Regulation of Mitosis. *Nature* **1996**, *380*, 544−547.
(71) Liou, Y. C.; Zhou, X. Z.; Lu, K. P. Prolyl Isomerase Pin1 as a Molecular Switch to Determine the Fate of Phosphoproteins. *Trends Biochem. Sci.* **2011**, *36*, 501−514.
(72) Lu, P.-J.; Zhou, X. Z.; Shen, M.; Lu, K. P. Function of Ww Domains as Phosphoserine-or Phosphothreonine-Binding Modules. *Science* **1999**, *283*, 1325−1328.
(73) Zhou, X. Z.; Kops, O.; Werner, A.; Lu, P.-J.; Shen, M.; Stoller, G.; Küllertz, G.; Stark, M.; Fischer, G.; Lu, K. P. Pin1-Dependent Prolyl Isomerization Regulates Dephosphorylation of Cdc25c and Tau Proteins. *Mol. Cell* **2000**, *6*, 873−883.
(74) Ranganathan, R.; Lu, K. P.; Hunter, T.; Noel, J. P. Structural and Functional Analysis of the Mitotic Rotamase Pin1 Suggests Substrate Recognition Is Phosphorylation Dependent. *Cell* **1997**, *89*, 875−886.
(75) Verdecia, M. A.; Bowman, M. E.; Lu, K. P.; Hunter, T.; Noel, J. P. Structural Basis for Phosphoserine-Proline Recognition by Group IV WW Domains. *Nat. Struct. Biol.* **2000**, *7*, 639−643.
(76) Zhang, M.; Wang, X. J.; Chen, X.; Bowman, M. E.; Luo, Y.; Noel, J. P.; Ellington, A. D.; Etzkorn, F. A.; Zhang, Y. Structural and Kinetic Analysis of Prolyl-Isomerization/Phosphorylation Cross-Talk in the Ctd Code. *ACS Chem. Biol.* **2012**, *7*, 1462−1470.
(77) Jacobs, D. M.; Saxena, K.; Vogtherr, M.; Bernado, P.; Pons, M.; Fiebig, K. M. Peptide Binding Induces Large Scale Changes in Inter-Domain Mobility in Human Pin1. *J. Biol. Chem.* **2003**, *278*, 26174−26182.
(78) Matena, A.; Sinnen, C.; van den Boom, J.; Wilms, C.; Dybowski, J. N.; Maltaner, R.; Mueller, J. W.; Link, N. M.; Hoffmann, D.; Bayer, P. Transient Domain Interactions Enhance the Affinity of the Mitotic Regulator Pin1 toward Phosphorylated Peptide Ligands. *Structure* **2013**, *21*, 1769−1777.
(79) Namanja, A. T.; Peng, T.; Zintsmaster, J. S.; Elson, A. C.; Shakour, M. G.; Peng, J. W. Substrate Recognition Reduces Side-Chain Flexibility for Conserved Hydrophobic Residues in Human Pin1. *Structure* **2007**, *15*, 313−327.
(80) Wilson, K. A.; Bouchard, J. J.; Peng, J. W. Interdomain Interactions Support Interdomain Communication in Human Pin1. *Biochemistry* **2013**, *52*, 6968−6981.
(81) Wang, X.; Mahoney, B. J.; Zhang, M.; Zintsmaster, J. S.; Peng, J. W. Negative Regulation of Peptidyl-Prolyl Isomerase Activity by Interdomain Contact in Human Pin1. *Structure* **2015**, *23*, 2224−2233.
(82) Guo, J.; Zhou, H. X. Dynamically Driven Protein Allostery Exhibits Disparate Responses for Fast and Slow Motions. *Biophys. J.* **2015**, *108*, 2771−2774.
(83) Namanja, A. T. *Molecular Basis for Signal Transduction in the Bimodular Cell-Cycle Enzyme Pin1*. Ph.D. Dissertation, University of Notre Dame, 2009.
(84) Myers, R. S.; Jensen, J. R.; Deras, I. L.; Smith, J. L.; Davisson, V. J. Substrate-Induced Changes in the Ammonia Channel for Imidazole Glycerol Phosphate Synthase. *Biochemistry* **2003**, *42*, 7013−7022.
(85) Douangamath, A.; Walker, M.; Beismann-Driemeyer, S.; Vega-Fernandez, M. C.; Sterner, R.; Wilmanns, M. Structural Evidence for Ammonia Tunneling across the $(\beta\alpha)_8$ Barrel of the Imidazole Glycerol Phosphate Synthase Bienzyme Complex. *Structure* **2002**, *10*, 185−193.
(86) Kazi, R.; Dai, J.; Sweeney, C.; Zhou, H. X.; Wollmuth, L. P. Mechanical Coupling Maintains the Fidelity of NMDA Receptor-Mediated Currents. *Nat. Neurosci.* **2014**, *17*, 914−922.
(87) Sharp, K.; Skinner, J. J. Pump-Probe Molecular Dynamics as a Tool for Studying Protein Motion and Long Range Coupling. *Proteins: Struct., Funct., Genet.* **2006**, *65*, 347−361.
(88) Tenboer, J.; Basu, S.; Zatsepin, N.; Pande, K.; Milathianaki, D.; Frank, M.; Hunter, M.; Boutet, S.; Williams, G. J.; Koglin, J. E.; et al. Time-Resolved Serial Crystallography Captures High-Resolution Intermediates of Photoactive Yellow Protein. *Science* **2014**, *346*, 1242−1246.
(89) Barends, T. R.; Foucar, L.; Ardevol, A.; Nass, K.; Aquila, A.; Botha, S.; Doak, R. B.; Falahati, K.; Hartmann, E.; Hilpert, M.; et al. Direct Observation of Ultrafast Collective Motions in CO Myoglobin Upon Ligand Dissociation. *Science* **2015**, *350*, 445−450.
(90) Pang, X.; Zhou, H. X. Disorder-to-Order Transition of an Active-Site Loop Mediates the Allosteric Activation of Sortase A. *Biophys. J.* **2015**, *109*, 1706−1715.
(91) Byeon, I. J.; Dao, K. K.; Jung, J.; Keen, J.; Leiros, I.; Doskeland, S. O.; Martinez, A.; Gronenborn, A. M. Allosteric Communication between cAMP Binding Sites in the RI Subunit of Protein Kinase a Revealed by NMR. *J. Biol. Chem.* **2010**, *285*, 14062−14070.
(92) McNicholl, E. T.; Das, R.; SilDas, S.; Taylor, S. S.; Melacini, G. Communication between Tandem cAMP Binding Domains in the Regulatory Subunit of Protein Kinase A-Iα as Revealed by Domain-Silencing Mutations. *J. Biol. Chem.* **2010**, *285*, 15523−15537.
(93) Gunasekaran, K.; Ma, B. Y.; Nussinov, R. Is Allostery an Intrinsic Property of All Dynamic Proteins? *Proteins: Struct., Funct., Genet.* **2004**, *57*, 433−443.
(94) Clarkson, M. W.; Gilmore, S. A.; Edgell, M. H.; Lee, A. L. Dynamic Coupling and Allosteric Behavior in a Nonallosteric Protein. *Biochemistry* **2006**, *45*, 7693−7699.
(95) Ludlow, R. F.; Verdonk, M. L.; Saini, H. K.; Tickle, I. J.; Jhoti, H. Detection of Secondary Binding Sites in Proteins Using Fragment Screening. *Proc. Natl. Acad. Sci. U.S.A.* **2015**, *112*, 15910−15915.
(96) Hilser, V. J.; Thompson, E. B. Intrinsic Disorder as a Mechanism to Optimize Allosteric Coupling in Proteins. *Proc. Natl. Acad. Sci. U.S.A.* **2007**, *104*, 8311−8315.
(97) Ferreon, A. C.; Ferreon, J. C.; Wright, P. E.; Deniz, A. A. Modulation of Allostery by Protein Intrinsic Disorder. *Nature* **2013**, *498*, 390−394.

DOI: 10.1021/acs.chemrev.5b00590
Chem. Rev. 2016, 116, 6503−6515